Well-Dispersed Chitosan/Graphene Oxide Nanocomposites

Xiaoming Yang,[†,‡] Yingfeng Tu,[†] Liang Li,[*,§,‡] Songmin Shang,[*,‡] and Xiao-ming Tao[‡]

College of Chemistry, Chemical Engineering and Materials Sciences, Soochow University, Suzhou 215123, China, Key Laboratory for Green Chemical Process of Ministry of Education, School of Materials Science and Engineering, Wuhan Institute of Technology, Wuhan 430073, China, and Institute of Textiles and Clothing, The Hong Kong Polytechnic University, Hong Kong, China

ABSTRACT Nanocomposites of chitosan and graphene oxide are prepared by simple self-assembly of both components in aqueous media. It is observed that graphene oxide is dispersed on a molecular scale in the chitosan matrix and some interactions occur between chitosan matrix and graphene oxide sheets. These are responsible for efficient load transfer between the nanofiller graphene and chitosan matrix. Compared with the pure chitosan, the tensile strength, and Young's modulus of the graphene-based materials are significantly improved by about 122 and 64%, respectively, with incorporation of 1 wt % graphene oxide. At the same time, the elongation at the break point increases remarkably. The experimental results indicate that graphene oxide sheets prefer to disperse well within the nanocomposites.

KEYWORDS: chitosan • graphene • nanocomposites • self-assembly

INTRODUCTION

Recently, more attention has been paid to natural polymers for sustainable development and environmental preservation (1). Chitosan, a copolymer of β[1,4]-linked 2-acetamido-2-deoxy-D-glucopyranose and 2-amino-2-deoxy-D-glucopyranose, is generally obtained by deacetylation of chitin, one of the most plentiful natural polymers on earth (2). Because of its good biocompatibility, biodegradability, and multiple functional groups, chitosan (CS) has attracted significant interest in a broad range of applications such as water treatment, separation membrane, food package, tissue engineering, and drug delivery (3). However, low mechanical properties of chitosan restrict its use in a wide-range application. Nanocomposite technology using nanofillers such as carbon nanotubes, clay, and hydroxyapatite at low loading has already been proven to be an effective way to cope with the problems (4−6). When the nanofillers are dispersed homogeneously, or best on the molecular scale, in the chitosan matrix, maximal mechanical enhancement can just be achieved. At present, carbon nanotubes as one-dimensional nanomaterials are considered to be an ideal reinforcing agent for polymer matrix because of their unique structure and properties (7). However, the expensive multistep methods used to prepare and purify carbon nanotubes, the intrinsic bundling of carbon nanotubes limit their applications on an industrial scale.

On the other hand, a two-dimensional single-layered graphene, the basic building block for naturally occurring graphite, have currently attracted tremendous attention especially because of their low cost, unique structure, and extraordinary electronic and mechanical properties (8−10). As in the case of carbon nanotubes, processing and dispersion of graphene materials including graphene oxide (GO) in the polymeric hosts constitutes the main challenge before implementation of high-performance graphene-based nanocomposites. The intrinsic van der Waals interactions between layers of graphene easily results in agglomeration, which leads to insolubility as occurs in carbon nanotubes. The occurrence of such agglomerations inevitably lower the reinforcement effectiveness of nanofillers, because the maximal load transfer and lowest filler loading can only be attained when the nanofillers are dispersed on the molecular scale in the polymer matrix. If the nanofillers in the polymer matrix could be dispersed on a molecular scale and interacted with the matrix by chemical bonding or strong intermolecular forces, significant improvements in the mechanical properties of the material or unexpected new properties might be achieved. These chemical functionalizations have been found to be a feasible and effective way for improving the dispersion of graphene materials and interfacial bonding between the graphene and the matrix (11−13).

It is crucial to have the uniform filler dispersion within the polymer matrix and good interfacial adhesion between nanofillers and polymer matrix. In the family of graphene, GO attaches many oxygen-containing hydrophilic functional groups such as −COOH and −OH (14−16). Moreover, the surfaces of GO sheets are highly negatively charged when dispersed in water, apparently as a result of ionization of carboxylic acid and phenolic hydroxyl groups on the GO sheets (17). The hydrophylicity of GO and electrostatic

* Corresponding author. E-mail: msell08@163.com (L.L.); tcshang@inet.polyu.edu.hk (S.S.).
Received for review March 14, 2010 and accepted June 01, 2010
† Soochow University.
‡ The Hong Kong Polytechnic University.
§ Wuhan Institute of Technology.
DOI: 10.1021/am100222m

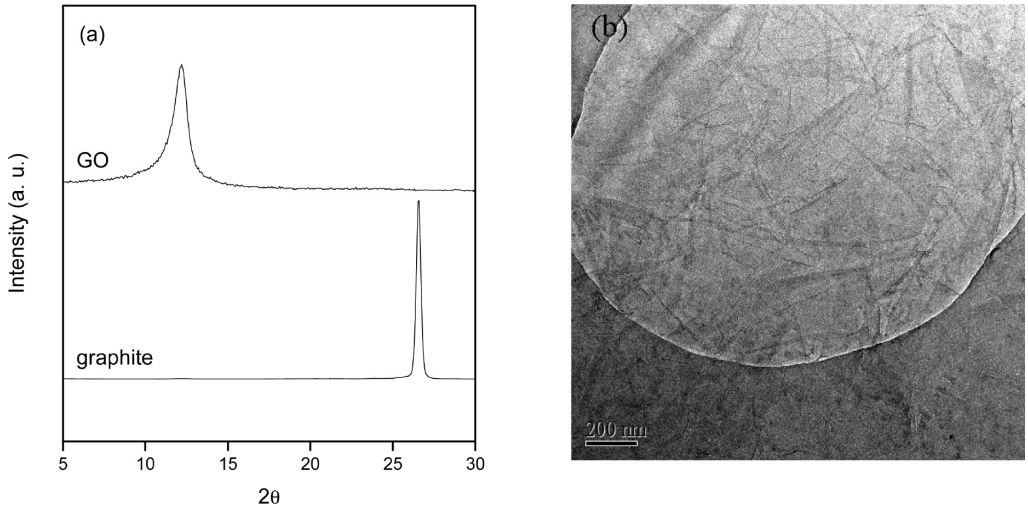

FIGURE 1. (a) XRD patterns of graphite and GO, and (b) TEM image of GO.

repulsion results in the dispersion of GO at the individual sheet level in water. On the other hand, as a hydrophilic biopolymer with $-NH_2$ and $-OH$ in each unit, CS can be protonated to polycationic material in acid media, which is favor of the interaction between polymer chains and GO sheets. Thus a good dispersion of GO in CS solution is expected. Here we report a simple and environmentally friendly strategy for the synthesis of CS/GO nanocomposites by self-assembly. The tensile strength and Young's modulus are significantly improved by about 122 and 64%, respectively, by addition of only 1 wt % GO.

EXPERIMENTAL SECTION

Materials. Chitosan (CS) was supplied by Shandong Chitin Powder Factory (China). It has a degree of deacetylation of 95% and viscosity-average molecular weight of 600,000 g/mol. Graphite powder was purchased from Uni-Chem. Other reagents were of analytical grade and used without further purification.

Synthesis of CS/GO Nanocomposites. Graphene oxide (GO) was prepared from graphite by the Hummers method (18, 19). CS/GO nanocomposites with 0.3, 0.5, and 1 wt % of filler were prepared as follows: GO was dissolved in 20 mL of water and treated with ultrasound for 45 min. CS solution of 1 wt % was prepared by dissolving CS in 0.5% (v/v) aqueous acetic acid solution. Then GO solution was added into the chitosan solution, followed by stirring for 24 h. After that, this homogeneous CS/GO solution was poured into a hydrophobic glass plate kept at 40 °C for film formation until its weight equilibrated.

Characterization. Transmission electron microscopy (TEM) measurements were conducted on a JEM-200CX transmission electron microscope with an accelerating voltage of 200 kV. The thin setion samples were prepared using microtomed. The failure surface of the CS/GO nanocomposite film (after tensile tests) was observed via scanning electron microscopy (SEM, JEOL model JSM-6490). The failure surfaces were coated with gold before analysis. X-ray diffraction (XRD) patterns were obtained on PHILIPS PW 3710 diffractometer using Cu Kα radiation source at room temperature. Fourier-transform infrared spectra (FTIR) spectra were recorded on a Perkin-Elmer spectrum 100 FT-IR spectrometer. Differential scanning calorimetry (DSC) measurements were performed on a Perkin-Elmer Diamond. DSC traces of each film were obtained from the second heating run at a constant rate of 20 K/min, after the first run of heating to 190 °C and cooling naturally to room temperature under nitrogen atmosphere. The tensile strength, elongation, and Young's modulus of CS/GO nanocomposites were measured on a universal tensile testing machine (Instron 4411) at 20 °C with 60% relative humidity. The extension rate was 5 mm/min and the load cell was 250 N with a gauge length of 40 mm. The specimen dimension was 60 mm in length, 10 mm in width, and 0.04 mm in thickness. Five parallel measurements were carried out for each sample. X-ray photoelectron spectrometer (XPS) (KRATOS Analytical) with a monochromated Mg Kα radiation of 1253.6 eV was used for elemental analyses of GO. Atomic force microscope (AFM) images were obtained using a MultiMode V microscope. AFM samples were prepared by coating the GO on newly cleaved mica surfaces.

RESULTS AND DISCUSSION

In a typical preparation, GO was synthesized from graphite powder by a Hummers method (18, 19). X-ray diffraction (XRD) patterns of the parent graphite and GO (Figure 1a) show the transformation of the interlayer spacing, which is a clear indication of the complete transformation from graphite to GO. As shown in Figure 1b, transmission electron microscopy (TEM) images show that graphene was fully exfoliated into individual sheets in water by ultrasonic treatment (20, 21). The AFM image and its corresponding height profiles (Figure 2), show that GO sheets on a silica surface are flat (0.851 nm thick). This observation confirms that the GO sheets are dispersed uniformly in water.

Well-dispersed CS/GO nanocomposites were fabricated through a simple self-assembly method by solution mixing as described in the experimental section. GO can be dispersed very well in water at the level of individual sheets because of the many oxygen-containing functional groups on the surfaces of GO and electrostatic repulsion between the negative charge of GO sheets. Furthermore, because of the many amino and hydroxyl groups in the unit of CS and the polycationic nature of CS in acid media, electrostatic attraction and hydrogen bonding between CS and GO are potentially achievable and could induce the truly homogeneous codispersion of CS and GO on the molecular scale and enhance interfacial adhesion as well as mechanical performance of the nanocomposite (22).

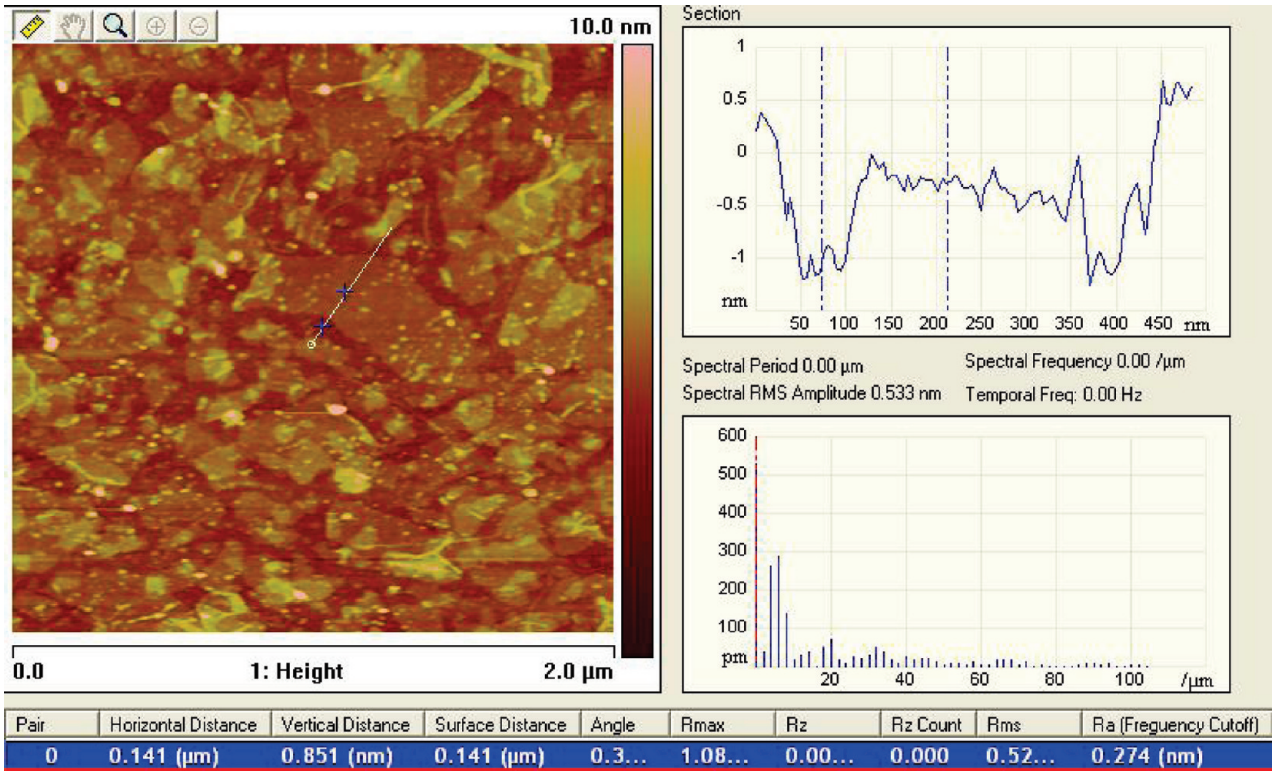

FIGURE 2. AFM image and its height profiles of GO sheets.

To determine the quality of the nanofiller dispersion in CS, scanning electron microscopy (SEM) was employed. Figure 3 shows SEM images of CS/GO nanocomposites with different GO loadings (0.3 wt %, 1 wt %). The SEM images of 0.5 wt % is like the 1 wt %. From the images of film surfaces (Figure 2a–c), no obvious difference between pure CS and CS/GO nanocomposites can be observed. It shows the well-dispersed status of GO in the CS matrix without any aggregation, illustrating good adhesion between fillers and matrix. The dispersion state of GO sheets in CS matrix is much better than that of carbon nanotubes in CS matrix (23). More interestingly, the fracture surfaces of the CS/GO films after tensile testing are totally different with that of the pure CS, as shown in Figure 3d–g. They are also different with those of the CS/carbon nanotubes films (6). With the addition of GO, the fracture-surface images of the films exhibit a stack of sheets, just like that of the GO membranes (8, 24).

FTIR experiments were carried out to investigate the interaction between GO and CS. As shown in Figure 4, in the spectrum of GO, the peak at 1730 and 1630 cm^{-1} are characteristics of the C═O stretch of the carboxylic group on the graphene oxide and deformations of the O–H bond in water, respectively (25). In the spectrum of CS, there are two characteristic absorbance bands centered at 1651 and 1596 cm^{-1}, which correspond to the C═O stretching vibration of –NHCO– and the N–H bending of $-NH_2$, respectively. Compared with pure CS and GO, both peaks at 1596 cm^{-1} related to $-NH_2$ absorbance vibration and at 1730 cm^{-1} belonging to C═O stretch of the carboxylic group disappear in the spectra of CS/GO nanocomposites. Moreover, the band corresponding to the C═O characteristic stretching band of the amide group shifts to a lower wavenumber. These could be ascribed to the synergistic effect of hydrogen bonding between CS and the oxygenated groups in GO and electrostatic interaction between polycationic CS and the negative charge on the surface of GO.

Table 1. XPS Data (N1s) for CS and CS/GO 1 wt % Nanocomposite

sample	N1[a] (%)	N2[b] (%)	N3[c] (%)
CS	81.4	11.5	7.1
CS/GO 1 wt % nanocomposite	76.7	12.0	11.3

[a] 399.4 eV. [b] 400.5 eV. [c] 401.7 eV.

The XPS spectra of CS/GO 1 wt % nanocomposite (Figure 5) display no obvious changes in the C 1s spectrum in comparison to CS. However, there is a difference in N 1s spectrum. Figure 4 shows the XPS N 1s core-level spectra of CS and the CS/GO nanocomposite. The N 1s spectrum can be deconvoluted into three peak component with binding energies (BEs) at 399.4, 400.5, and 401.7 eV (26), attributed to the amine, amide, and the protonated amine species, respectively. In comparison with the N 1s spectrum of CS, that of the CS/GO nanocomposite in 401.7 eV increase from 7.1% to 11.3% (Table 1). The increase in the protonated amine provides the supporting formation of electrostatic interaction between the negative charge on the surface of GO and N groups of CS (27), which is consistent with FTIR data.

X-ray diffraction (XRD) patterns of the nanocomposites further determine that graphene-based sheets are indeed present as individual graphene sheets in the composites as shown in Figure 6. After GO is dispersed into the CS matrix, the XRD pattern of the CS/GO nanocomposites shows only

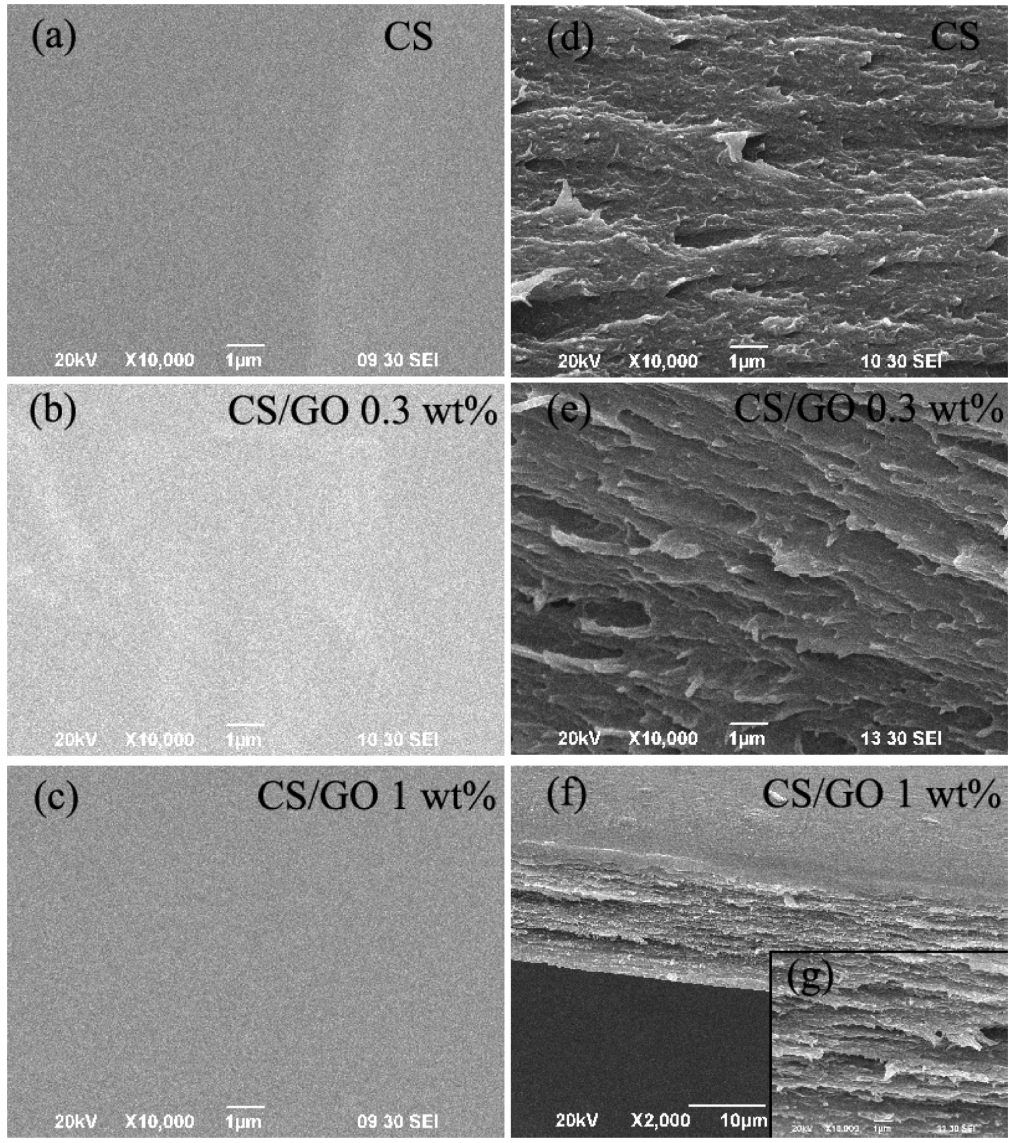

FIGURE 3. SEM film-surface images (a–c) and fracture-surface images (d–g) of CS and CS/GO nanocomposites. Image g is the magnification of f.

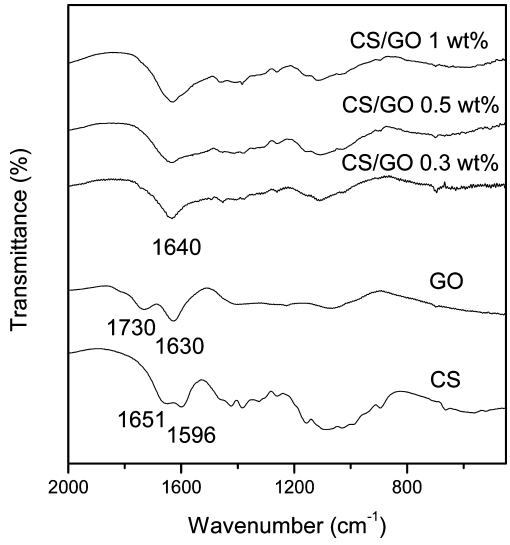

FIGURE 4. FTIR spectra of GO, CS, and their nanocomposites.

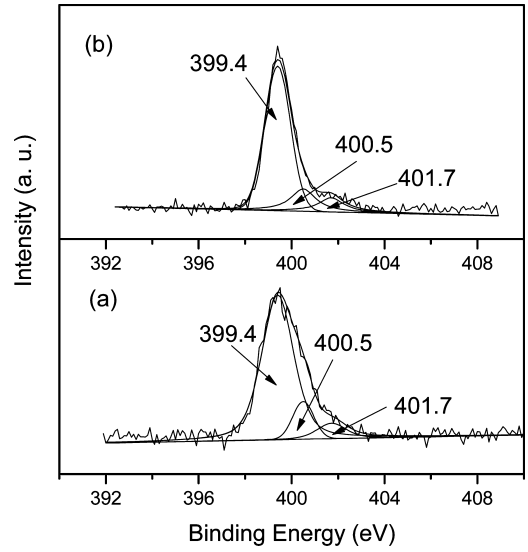

FIGURE 5. XPS N 1s core-level spectra of (a) CS and (b) the CS/GO 1 wt % nanocomposite.

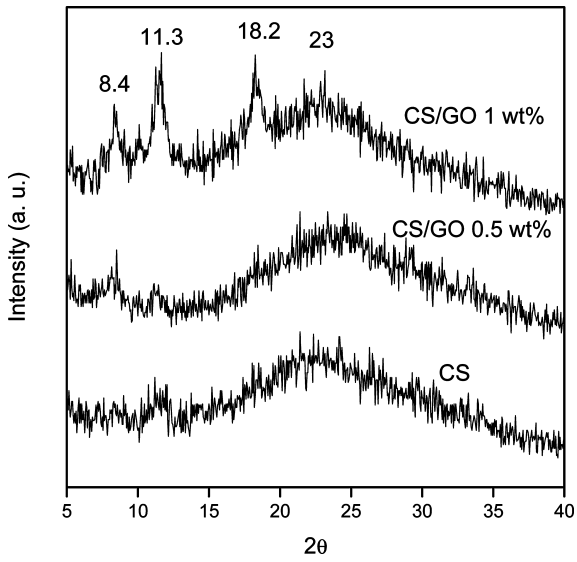

FIGURE 6. XRD patterns of CS and CS/GO nanocomposites.

the CS diffraction peaks from CS and the diffraction peak of GO (Figure 1a) disappears, which clearly demonstrate the formation of fully exfoliated structure of GO sheets in the polymer matrix and the disappearance of the regular and periodic structure of graphene (28). It is noticed that incorporation of less than 0.5 wt % GO only slightly increase the intensity of the characteristic peaks of CS. However, the intensity of the characteristic peaks of CS obviously increases with the loading of 1 wt % GO in the CS matrix, characteristic peaks of CS around $2\theta = 8.4$, 11.3, 18.2, and 23° can be clearly seen from Figure 6. The first two peaks correspond to the hydrated crystalline structure, whereas the broadened peak at about 23° indicates the existence of an amorphous structure (29, 30). A similar phenomenon also can be found in many polymer/carbon nanotubes nanocomposites and is considered to be a result of polymer crystallization that is induced by carbon nanotubes (31, 32). In this particular case, the electrostatic interaction and hydrogen bonding may contribute to a relatively ordered arrangement of the attached CS chains along the rigid template offered by GO.

The glass-transition temperature (T_g) of polymer is affected by the mobility of polymer chains. Differential scanning calorimetry (DSC) was used to investigate the T_g of the CS/GO nanocomposites. As shown in Figure 7, T_g of CS in the second scan is about 175.4 °C (33). With the addition of GO, it increases gradually to 180.4 °C. The increase in T_g can be ascribed to an effective attachment of CS to the GO sheets that constrains the segmental motion of the CS chains by hydrogen bonding and electrostatic attraction, as demonstrated in other reports (34, 35).

The mechanical behaviors of the films of the pure CS matrix as well as the CS/GO nanocomposites with various loadings of GO were investigated by tensile tests at 20 °C. The typical stress–strain curves of CS and the CS/GO nanocomposites are shown in Figure 8a. One can see that the addition of GO significantly improves the tensile properties of CS matrix. It is strongly evident that even a small amount of GO could significantly improve the mechanical properties. The tensile strength and Young's modulus increased sharply

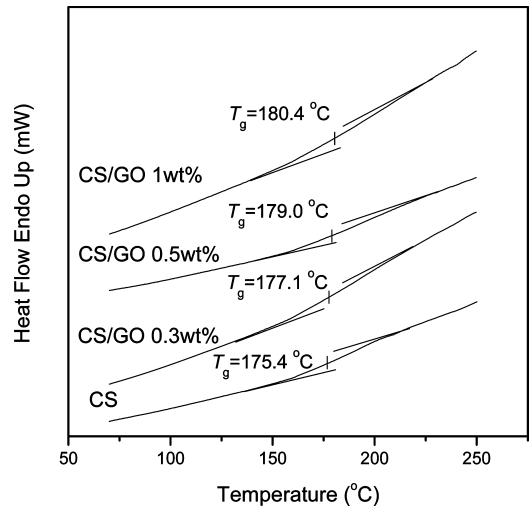

FIGURE 7. DSC traces of CS and CS/GO nanocomposites.

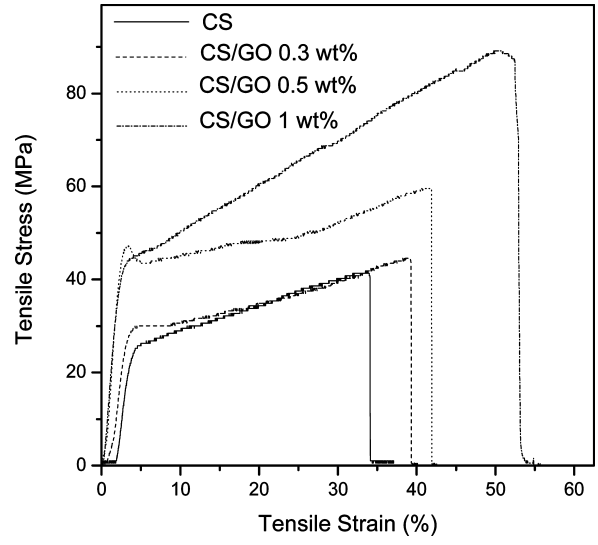

FIGURE 8. Stress–strain behaviors for the films of CS/GO nanocomposites with different GO loadings.

by 122% from 40.1 to 89.2 MPa (Figure 8a) and by 64% from 1.32 to 2.17 GPa (Figure 8b) with an increase in GO loading from 0 to 1 wt %, respectively. Furthermore, it is interesting to see that the CS/GO nanocomposites have not only higher strength but also a larger elongation than those corresponding pure CS, which is different with those in poly(vinyl alcohol)/GO nanocomposites (36) and CS/carbon nanotubes nanocomposites (6, 23). More specially, the elongation at the break point of the film with 1 wt % GO is about 88%, which is an increase of 159% in comparison of that of the pure CS film. In some cases, simultaneously improved strength and elongation of polymer nanocomposites have been reported, with incorporation of oriented or functionalized nanofillers (37, 38).

The addition of GO can affect the crystallinity of chitosan, as shown in XRD patterns in Figure 6, which is an important factor for the enhancement of tensile properties of polymer. It is worth noting that, though incorporation of less than 0.5 wt % GO only slightly affects the crystalline structure of CS, the significant increase of the strain modulus and Young's modulus of the films with less than 0.5 wt % GO is ac-

Scheme 1. Schematic Representation of the Well-Dispersed Nanocomposites

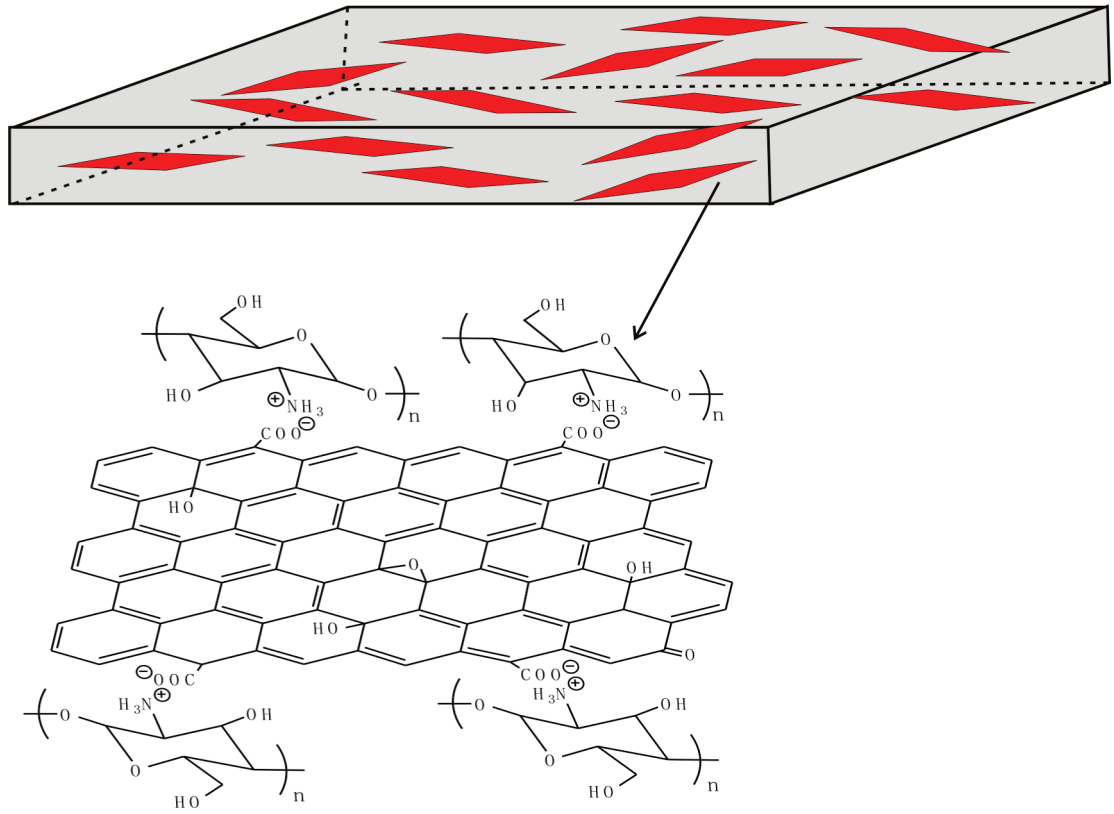

companied with an obvious increase of elongation at break. Obviously here the crystallinity plays a less important role in the further increase of the mechanical properties for CS/GO nanocomposites. Similar results have been demonstrated for carbon nanotube-based nanocomposites (22, 39), whereas the largest improvement in tensile strength and modulus is also observed for composites with 1 wt % GO, in which a great increased crystallinity of CS is also observed. The improved tensile properties are ascribed to both the interaction between GO and CS and the change of crystallinity. All results suggest preferential alignment of graphene oxide as schematically shown in Scheme 1. But additional work is needed to investigate it.

In general, good dispersion and interfacial stress transfer are important factors for preparing reinforcing nanocomposites. This leads to a more uniform stress distribution and minimizes the presence of the stress concentration center (7). As discussed above, the oxygen-containing groups and negative charges on the GO surface can interact effectively with the polycationic CS through hydrogen bonding and electrostatic attraction. Moreover, the large aspect ratio of the graphene sheets is also favorable to stress transfer. The compatibility and strong interaction between GO and the CS matrix greatly enhances the unidirectional dispersion of GO sheets on the molecular scale in CS matrix as well as the interfacial adhesion, thus significantly increasing the mechanical properties of the nanocomposites.

CONCLUSIONS

Biopolymer nanocomposites were prepared from CS as the matrix and GO as reinforcing nanofillers by a simple self-assembly strategy. A uniform distribution and fine dispersion for GO in CS matrix have been evidenced. The incorporation of only 1 wt % GO dramatically increases the tensile strength and Young's modulus by 122 and 64%, respectively, from 40.1 to 89.2 MPa and 1.32 to 2.17 GPa. Meanwhile, the elongation at the break point increases significantly. Our work demonstrates a good example for the preparation of high-performance polymer nanocomposites by using nanofiller graphene. And it can be expected that CS with largely improved mechanical properties may play a more important role in biochemical and electrochemical applications.

Acknowledgment. The work is supported by a grant (4-ZZ63) of The Hong Kong Polytechnic University, Key Project in Science & Technology Innovation Cultivation Program of Soochow University, Educational Bureau of Hubei Province (Q20091508), Scientific Research Foundation for Returned Overseas Chinese Scholars of MOE (20091341), Scientific Research Key Project of MOE (209081), and National Natural Science Foundation of China (20904044).

Supporting Information Available: Description of XPS C 1s core-level spectra of graphite and GO, additional TEM image of thin section of 1 wt % CS/GO film (PDF). This material is available free of charge via the Internet at http://pubs.acs.org.

REFERENCES AND NOTES

(1) Chabba, S.; Matthews, G. F.; Netravali, A. N. *Green. Chem.* **2005**, *7*, 576–581.
(2) Rinaudo, M. *Prog. Polym. Sci.* **2006**, *31*, 603–632.
(3) Kumar, M. *React. Funct. Polym.* **2000**, *46*, 1–27.
(4) Kim, S. B.; Kim, Y. J.; Yoon, T. L.; Park, S. A.; Cho, I. H.; Kim, E. J.; Kim, I. A.; Shin, J. W. *Biomaterials* **2004**, *25*, 5715–5723.

(5) Darder, M.; Colilla, M.; Ruiz-Hitzky, E. *Chem. Mater.* **2003**, *15*, 3774–3780.
(6) Wang, S. F.; Shen, L.; Zhang, W. D.; Tong, Y. J. *Biomacromolecules* **2005**, *6*, 3067–3072.
(7) Coleman, J. N.; Khan, U.; GunKo, K. *Adv. Mater.* **2006**, *18*, 689–706.
(8) Dikin, D. A.; Stankovich, S.; Zimney, E. J.; Piner, R. D.; Dommett, G. H. B.; Evmenenko, G.; Nguyen, S. T.; Ruoff, R. S. *Nature* **2007**, *448*, 457–460.
(9) Gomez-Navarro, C.; Burghard, M.; Kern, K. *Nano Lett.* **2008**, *8*, 2045–2049.
(10) Guo, H. L.; Wang, X. F.; Qian, Q. Y.; Wang, F. B.; Xia, X. H. *ACS. Nano.* **2009**, *3*, 2653–2659.
(11) Verdejo, R.; Barroso-Bujans, F.; Rodriguez-Perez, M. A.; Sajab, J. A.; Lopez-Manchado, M. A. *J. Mater. Chem.* **2008**, *18*, 2221–2226.
(12) Du, X.; Yu, Z. Z.; Dasari, A.; Ma, J.; Mo, M.; Meng, Y.; Mai, Y. W. *Chem. Mater.* **2008**, *20*, 2066–2068.
(13) Yang, Y.; Wang, J.; Zhang, J.; Liu, J.; Yang, X.; Zhao, H. *Langmuir* **2009**, *25*, 11808–11814.
(14) Stankovich, S.; Dikin, D. A.; Piner, R. D.; Kohlhaas, K. A.; Kleinhammes, A.; Jia, Y.; Wu, Y.; Nguyen, S. T.; Ruoff, R. S. *Carbon* **2007**, *45*, 1558–1565.
(15) Schniepp, H. C.; Li, J. L.; McAllister, M. J.; Sai, H.; Herrera-Alonso, M.; Adamson, D. H.; Prudhomme, R. K.; Car, R.; Saville, D. A.; Aksay, I. A. *J. Phys. Chem. B* **2006**, *110*, 8535–8539.
(16) Si, Y. C.; Samulski, E. T. *Nano Lett.* **2008**, *8*, 1679–1682.
(17) Li, D.; Muller, M. B.; Gilje, S.; Kaner, R. B.; Wallace, G. G. *Nature Nanotechnol.* **2008**, *3*, 101–105.
(18) Hummers, W. S.; Offeman, R. E., Jr. *J. Am. Chem. Soc.* **1958**, *80*, 1339.
(19) Ramanathan, T.; Abdala, A. A.; Stankovich, S.; Dikin, D. A.; Herrera-Alonso, M.; Piner, R. D.; Adamson, D. H.; Schniepp, H. C.; Chen, X.; Ruoff, R. S. *Nat. Nanotechnol.* **2008**, *3*, 327–331.
(20) Rafiee, J.; Rafiee, M.A.; Y, Z.Z.; Koratkar, N. *Adv. Mater.* **2010**, *22*, 1–4.
(21) Rafiee, M. A.; Rafiee, J.; Wang, Z.; Song, H.; Yu, Z. Z.; Koratkar, N. *ACS Nano* **2009**, *3*, 3884–3890.
(22) Liu, L. Q.; Barber, A. H.; Nuriel, S.; Wagner, H. D. *Adv. Funct. Mater.* **2005**, *15*, 975–980.
(23) Cao, X.; Dong, H.; Li, C. M.; Lucia, L. A. *J. Appl. Polym. Sci.* **2009**, *113*, 466–472.
(24) Chen, C.; Yang, Q. H.; Yang, Y.; Lv, W.; Wen, Y.; Hou, P. X.; Wang, M.; Cheng, H. M. *Adv. Mater.* **2009**, *21*, 3007–3011.
(25) Han, Y.; Lu, Y. *Compos. Sci. Technol.* **2009**, *69*, 1231–1237.
(26) Moulder, J. F.; Stickle, W. F.; Sobol, P. E.; Bomben, K. D. In *X-ray Photoelectron Spectroscopy*; Chastain, J., Ed.; Perkin-Elmer: Eden Prairie, MN, 1992.
(27) Compton, O. C.; Dikin, D. A.; Putz, K. W.; Brnson, L. C.; Nguyen, S. T. *Adv. Mater.* **2010**, *22*, 892–896.
(28) Du, X. S.; Xiao, M.; Meng, Y. Z.; Hay, A. S. *Carbon* **2005**, *43*, 195–197.
(29) Jaworska, M.; Sakurai, K.; Gaudon, P.; Guibal, E. *Polym. Int.* **2003**, *2*, 198–205.
(30) Rhim, J. W.; Hong, S. I.; Park, H. M.; Ng, P. K. *J. Agric. Food Chem.* **2006**, *54*, 5814–5822.
(31) Probst, O.; Moore, E. M.; Resasco, D. E.; Grady, B. P. *Polymer* **2004**, *45*, 4437–4443.
(32) Grady, B. P.; Pompeo, F.; Shambaugh, R. L.; Resasco, D. E. *J. Phys. Chem. B* **2002**, *106*, 5852–5858.
(33) Mucha, M.; Pawlak, A. *Thermochim. Acta* **2005**, *427*, 69–76.
(34) Leszczynska, A.; Pielichowski, K. *J. Therm. Anal. Calorim.* **2008**, *93*, 677–687.
(35) Yao, Z. L.; Braidy, N.; Botton, G. A.; Adronov, A. *J. Am. Chem. Soc.* **2003**, *125*, 16015–16024.
(36) Liang, J.; Huang, Y.; Zhang, L.; Wang, Y.; Ma, Y.; Guo, T.; Chen, Y. *Adv. Funct. Mater.* **2009**, *19*, 2297–2302.
(37) Gorga, R. E.; Cohen, R. E. *J. Polym. Sci., Part B: Polym. Phys.* **2004**, *42*, 2690–2702.
(38) Blond, D.; Barron, V.; Ruether, M.; Ryan, K. P.; Nicolosi, V.; Coleman, J. N. *Adv. Funct. Mater.* **2006**, *16*, 1608–1614.
(39) Zhang, X. F.; Liu, T.; Sreekumar, T. V.; Kumar, S.; Moore, V. C.; Hauge, R. H.; Smalley, R. E. *Nano Lett.* **2003**, *3*, 1285–1288. Zhao, X.; Zhang, Q.; Chen, D.; Lu, P. *Macromolecules* **2010**, *43*, 2357–2363.

AM100222M